4-1-2008

Geotail and LFM comparisons of plasma sheet climatology: 2. Flow variability

T. B. Guild

Harlan E. Spence
Boston University, harlan.spence@unh.edu

E. L. Kepko

V. Merkin

J. G. Lyon

See next page for additional authors

Authors

T. B. Guild, Harlan E. Spence, E. L. Kepko, V. Merkin, J. G. Lyon, M. Wiltberger, and C. C. Goodrich

Geotail and LFM comparisons of plasma sheet climatology: 2. Flow variability

Timothy B. Guild,[1,2] Harlan E. Spence,[1] E. Larry Kepko,[1] Viacheslav Merkin,[1] John G. Lyon,[1,3] Michael Wiltberger,[4] and Charles C. Goodrich[1]

[1]   We characterize the variability of central plasma sheet bulk flows with a 6-year Geotail data set and a 2-month Lyon-Fedder-Mobarry (LFM) global MHD simulation at two spatial resolutions. Comparing long databases of observed and simulated parameters enable rigorous statistical tests of the model's ability to predict plasma sheet properties during routine driving conditions and represent a new method of global MHD validation. In this study, we use probability density functions (PDFs) to compare the statistics of plasma sheet velocities in the Geotail observations with those in the LFM simulations. We find that the low-resolution model grossly underestimates the occurrence of fast earthward and tailward flows. Increasing the simulation resolution inherently changes plasma sheet mass transport in the model, allowing the development of fast, bursty flows. These flows fill out the wings of the velocity distribution and bring the PDF into closer agreement with observations.

Citation: Guild, T. B., H. E. Spence, E. L. Kepko, V. Merkin, J. G. Lyon, M. Wiltberger, and C. C. Goodrich (2008), Geotail and LFM comparisons of plasma sheet climatology: 2. Flow variability, *J. Geophys. Res.*, *113*, A04217, doi:10.1029/2007JA012613.

1.   Introduction

[2]   The Earth's plasma sheet is an important link in the solar-terrestrial system. As such, it has been the subject of many investigations characterizing its average properties [e.g., *Baumjohann et al.*, 1989; *Angelopoulos et al.*, 1993; *Huang and Frank*, 1994; *Kaufmann et al.*, 2004] and how those properties vary with the incident solar wind [e.g., *Tsyganenko and Mukai*, 2003; *Borovsky et al.*, 1998; *Wang et al.*, 2006] or substorm phase [e.g., *Nagai et al.*, 1998; *Machida et al.*, 1999; *Miyashita et al.*, 1999]. Since the plasma sheet plays a significant role in transporting solar wind plasma and energy deep into the inner magnetosphere, understanding its velocity structure is central to characterizing the nature of mass, momentum, and energy transport throughout the magnetosphere.

[3]   The large plasma sheet volume is relatively far from the Earth, frustrating investigations which attempt to study its global, time-dependent properties with orbiting spacecraft. The plasma sheet extends from nightside geosynchronous orbit to many tens of R_E antisunward and covers ∼30 R_E of cross-tail width. Spacecraft require long orbital periods to reach the majority of the plasma sheet and only sample one trajectory in time/space through its large volume

upon each traversal. Accordingly, statistical investigations must accumulate a global picture of the plasma sheet over years of spacecraft orbits, at the expense of short-term dynamics. This observational constraint will most likely remain until the launch of a constellation-class mission to the magnetotail, at least a decade from now by optimistic estimates.

[4]   Recent advances in the speed and scale of computational resources have recently enabled global MHD models to reach new levels of resolution and complexity. Global MHD models of the magnetosphere now routinely simulate day to week-long intervals using observed solar wind inputs, and researchers compare the simulation solutions to in situ magnetospheric measurements. While we lack global observational coverage of the dynamic plasma sheet, we can use global MHD simulations to investigate the multiscale fluid nature of plasma sheet dynamics. These models are tools to understand dynamics, however, only to the extent that they are successfully validated against observations in the plasma sheet.

[5]   In this study, we extend a companion work [*Guild et al.*, 2008] that compared the averaged Geotail plasma sheet observations with the average behavior of an LFM simulation in the plasma sheet. We refer to these long duration time averages of plasma sheet parameters as "climate," analogous with long-term average terrestrial weather patterns. Climate equally refers to the underlying variability of the parameters which contribute to those long-term averages, so in this paper we look closer at the distributions which made up the average plasma sheet velocity comparisons in the work of *Guild et al.* [2008]. Specifically, we compare velocity distributions observed by the Geotail spacecraft during a 2-month interval in 1996 with the

---

velocity distributions within an LFM simulation of those same 2 months to validate the LFM global MHD model with observations in the plasma sheet. Flow distributions span the range of continuously evolving conditions from typical to extreme levels of activity within the bimodal plasma sheet [*Kennel*, 1995], thereby providing a rigorous test of model performance. Velocity distributions are the most physically meaningful measure of plasma sheet variability encompassed in the data sets used in these companion studies (compared to density, thermal energy, or thermal pressure variability). Additionally, there already exists a significant body of literature devoted to the analysis methods and theories underlying flow distributions in plasmas from which we can draw expertise or interpretation. This systematic validation effort characterizes model strengths, suggests improvements based on model weaknesses, and represents an important step toward transitioning codes from research tools to mature, operational forecasting models.

2. Observations

[6] We used Geotail data from the Low Energy Particle (LEP) [*Mukai et al.*, 1994] and Magnetic Field (MGF) [*Kokubun et al.*, 1994] experiments, available through the DARTS/GEOTAIL online database, to characterize the properties of the plasma sheet. The LEP experiment measures ions from 7 eV/charge to 42 keV/charge, and the DARTS database provides moments of the ion distributions at 12-s cadence. In this study we are interested in bulk transport through the plasma sheet, so we used only ion data from the LEP experiment as ions carry most of the mass, momentum, and energy. The MGF experiment uses dual three-axis fluxgate magnetometers to provide magnetic field measurements at a 3-s cadence. We merged these data sets by linearly interpolating to a common 12-s timescale. In total, we used Geotail data from January 1995 through December 2000, when Geotail was in an $\sim 10 \times 30\ R_E$, 5.4-d orbit. The majority of this investigation, however, focuses on the 2-month interval from 23 February through 25 April 1996 when Geotail predominantly sampled the premidnight sector of the geomagnetic tail.

3. Simulations

[7] We compared the Lyon-Fedder-Mobarry (LFM) global MHD simulation to the Geotail data described in section 2. The LFM model solves the three-dimensional ideal MHD equations self-consistently on a roughly cylindrical grid in geospace, organized in stretched, spherical computational coordinates. The simulation domain extends from about 30 R_E upstream of the Earth to $\sim 300\ R_E$ downstream, and $\sim 100\ R_E$ in both the Y_{SM} and Z_{SM} directions. The model takes observed solar wind inputs at the upstream boundary and couples to a simple two-dimensional height-integrated ionospheric model at the 2.1 R_E inner boundary. A comprehensive discussion of the LFM model is given in the work of *Lyon et al.* [2004].

[8] WIND observations for the interval between 23 February and 25 April 1996, defined the driving boundary conditions for this LFM simulation. We show these model inputs in Figure 1 where we plot, from top to bottom, the solar wind

number density (#/cm^3), speed (km/s), ram pressure (nP), IMF $B_{Y,GSM}$ (nT) and $B_{Z,GSM}$ (nT), and B_{total} (nT). The solar wind speed, ram pressure, B_Z, and B_{total}, when averaged over the entire interval, are $\langle V_{SW} \rangle$ = 436 km/s, $\langle P_{RAM} \rangle$ = 2.1 nPa, $\langle B_Z \rangle$ = −0.48 nT, and $\langle |B| \rangle$ = 3.4 nT. We split the 2 month duration into nine subintervals for ease of running the simulations, and due to two WIND perigee passes near 27 March and 18 April, marked by the large gaps in Figure 1. Other, smaller gaps in the input time series correspond to times between individual simulations. We set the input B_X to zero in the simulation coordinates to avoid numerical complications at the upstream boundary of the grid. This is generally justifiable because the X_{SM} field component is not appreciably compressed across the subsolar bow shock and plays a minimal role in solar wind-magnetosphere coupling [*Lyon et al.*, 2004]. The LFM model solves the MHD equations with an internal cadence of ~ 0.2 s, but we exported the simulation magnetospheric and ionospheric variables every ~ 1.5 min, sufficient to obtain good statistics of the shortest duration velocity signatures typical of the simulated plasma sheet.

4. Comparison Time Series

[9] To assess the performance of the LFM for this interval, we flew a "virtual" Geotail spacecraft through the simulation volume and interpolated the LFM solution at the locations and times of Geotail's orbit. This analysis was facilitated with the CISM-DX software package [*Wiltberger et al.*, 2005]. We compare in Figure 2 our simulated time series (in blue) with the observed Geotail measurements (in red) throughout the 2-month interval. From top to bottom, we plot data/model comparisons of the logarithm of plasma number density (log(n); cm^{-3}), the bulk speed in the X_{GSM} direction (V_X; km/s), the total bulk speed ($|V|$; km/s), the logarithm of thermal energy (log(T); keV), and the total magnetic field ($|B|$; nT). The simulation thermal energy was derived from the pressure to density ratio. Again, the time series gaps indicate periods which were not simulated. The V_X component, in the second panel, most clearly shows the satellite transition from fast negative solar wind to slow, highly variable magnetospheric flow each time Geotail entered the magnetosphere. The satellite traversed the geomagnetic tail 10 times, predominantly in the premidnight sector between 14 and 23 R_E tailward of the Earth. During these tail passes, the satellite encountered shocked, dense solar wind in the magnetosheath, low density tail lobes, and the high density, hot plasma of the plasma sheet. To better understand the characteristics of the plasma sheet, we identified and included only observations that satisfy criteria representative of the central plasma sheet for the remainder of the study.

5. Plasma Sheet Selection

[10] We limited the data set selection to only plasma sheet measurements by adopting four criteria taken to be representative of the central plasma sheet and applying these selection rules to both the Geotail and LFM time series shown in Figure 2. We first included only measurements tailward of X_{GSM} = −10 R_E, ensuring observations within a tail-like field configuration. Second, we required the ther-
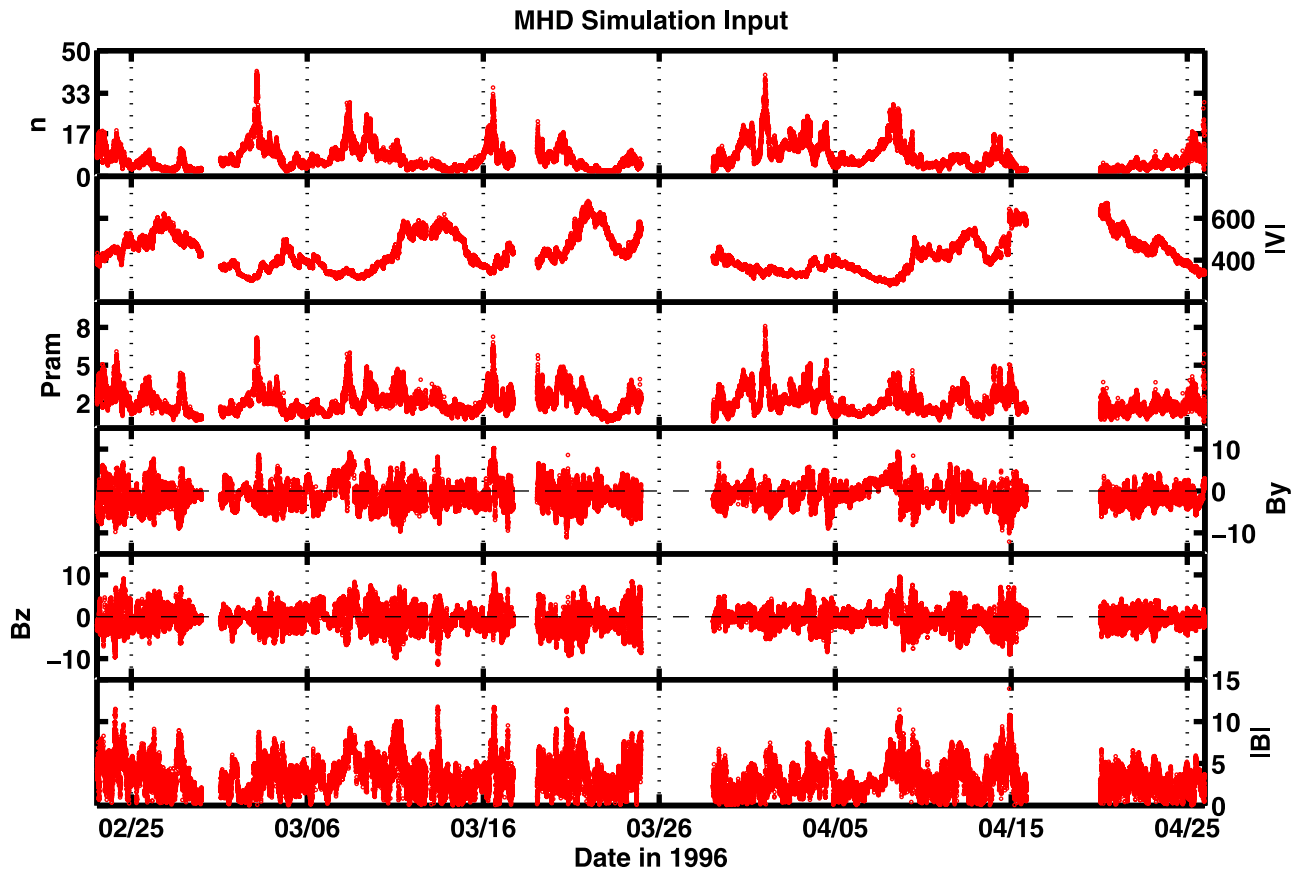
MHD Simulation Input

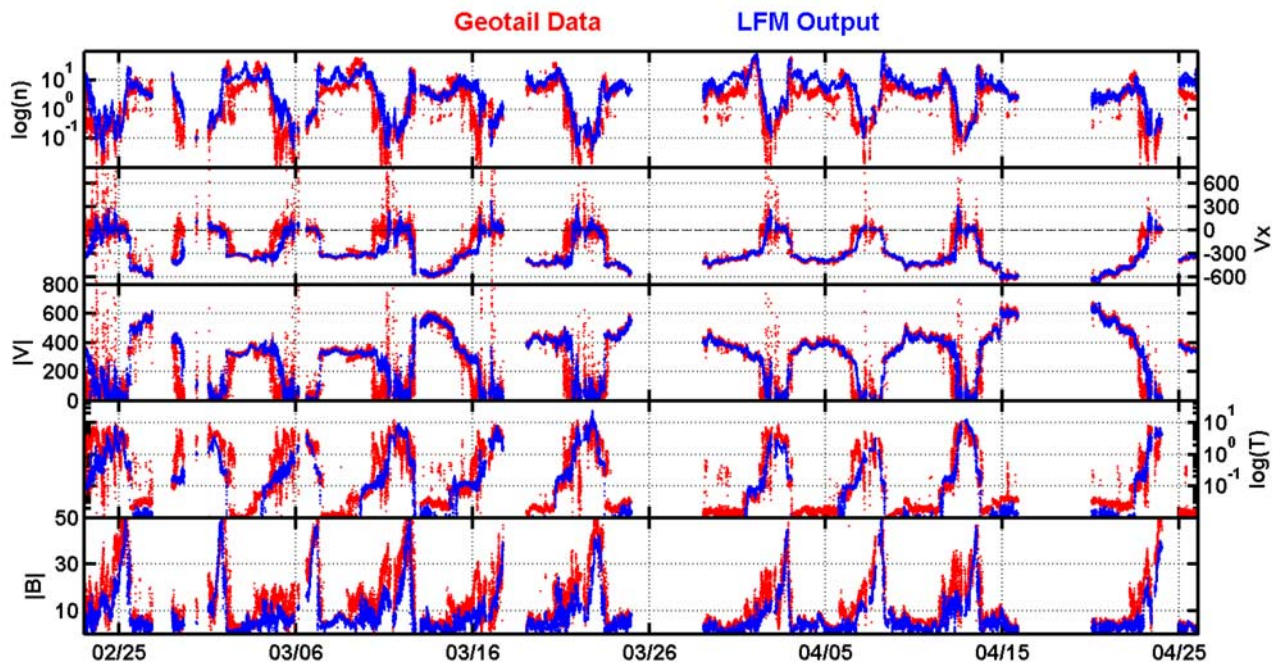**Figure 1.** Solar wind inputs to the LFM model during the 2-month simulation.

Figure 2. Time series of the Geotail satellite (red) and the LFM solution at the location of Geotail for the interval 23 February 1996 through 25 April 1996.

Table 1. Central Plasma Sheet Criteria for the Geotail and LFM Studies

Variable	Value
X_{GSM}	$< -10\ R_E$
T	> 1 keV
β	> 0.5
$\dfrac{B_Z}{B_{XY}}$	> 0.5[a]

[a]After *Baumjohann et al.* [1990].

mal energy to be larger than 1 keV. We determine the ion thermal energy from LEP data by averaging two diagonal components of the temperature tensor provided by the DARTS database ($kT_{Geotail} = \dfrac{k\left(T_{yy}+T_{zz}\right)}{2}$), and calculated the LFM plasma thermal energy by taking the pressure to density ratio. Third, we included only samples with a plasma $\beta > 0.5$, where β is the ratio of thermal to magnetic pressure. This limit bounds the thermally dominated region closest to the current sheet. Finally, we selected those samples close to the neutral sheet as measured by the magnetic field elevation angle, measured north or south from the equatorial *GSM* plane. We include only samples where $\dfrac{|B_z|}{B_{xy}} > 0.5$, corresponding to all elevation angles $> 26°$. Table 1 summarizes these criteria, which are adopted from many previous studies of the plasma sheet [e.g., *Baumjohann et al.*, 1990; *Angelopoulos et al.*, 1994; *Nishida et al.*, 1995; *Nagai et al.*, 1998]. By using such strict inclusion criteria, we ensured high confidence that our plasma sheet databases were not contaminated by inappropriate samples.

[11] Having defined the plasma sheet in our study, we used these criteria to extract only central plasma sheet observa-

tions from the Geotail and LFM time series in Figure 2. According to our definition, the Geotail spacecraft encountered the central plasma sheet only 4.4% of the time, for 2.3 cumulative days over the course of the 2 month interval. The virtual Geotail spacecraft encountered the LFM central plasma sheet only 7.1% of the time, for a total of 3.7 d. This underscores the reason why global plasma sheet data sets require many years of observations to accumulate sufficient coverage. Our plasma sheet databases included 10 independent satellite passes, and each pass generally observed the plasma sheet for many tens to hundreds of autocorrelation times, found by *Borovsky et al.* [1997] to be ~2 min. We use only this reduced central plasma sheet data set hereafter.

6. Comparison PDFs

6.1. PDFs for 2 Months at Geotail Location

[12] Probability density functions (PDFs) effectively capture the average values, maximum excursions, and variability inherent in a data set. PDFs have been employed to characterize the turbulent properties of the solar wind [e.g., *Sorriso-Valvo et al.*, 1999] and of geomagnetic indices [e.g., *Hnat et al.*, 2003] and to quantify the occurrence frequency of plasma sheet flow speeds [e.g., *Borovsky et al.*, 1997; *Angelopoulos et al.*, 1999]. *Angelopoulos et al.* [1999] used PDFs to demonstrate that magnetotail flows exhibit intermittent turbulence.

[13] In this section we use PDFs to compare statistical properties of plasma sheet flows observed by Geotail and simulated by the LFM. In Figure 3 we plot the PDFs of observed (red) and simulated (blue) velocities in the X_{GSM} direction from $-500 < V_X < +500$ km/s from the 2-month simulated interval described in section 3. We used velocities
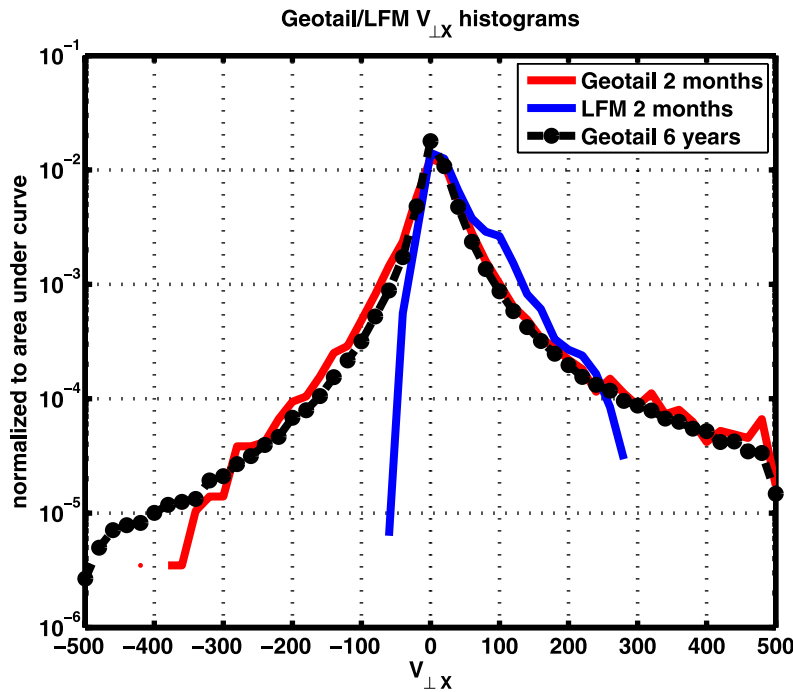

Figure 3. Probability density functions of 6 years of Geotail plasma sheet observations (dotted black line), 2 months of Geotail plasma sheet observations (red line), and 2 months of LFM simulation results at the Geotail orbit. Note the similarity between the long and short Geotail study, and the lack of fast LFM flows.

perpendicular to the instantaneous magnetic field (designated $V_\perp$) to estimate bulk convective transport. In addition to both 2-month PDFs, we also plot the PDF of Geotail flows in the central plasma sheet from the entire 6-year data set as a dotted black line. This longer data set uniformly sampled the entire plasma sheet and included far more data points for better statistics. The solar wind conditions during these 6 years were statistically similar to the solar wind driving the simulation for these 2 months; this property is demonstrated in a companion paper [*Guild et al.*, 2008]. We therefore consider this long data set more representative of the true statistical nature of plasma sheet velocities, including those larger velocities which occur at much lower frequencies. All PDFs shown in Figure 3 are determined using 20 km/s velocity bins and are normalized to the area under their curves, thus representing the relative occurrence frequency of observing flows of a certain speed in the plasma sheet.

[14] Both PDFs calculated from the Geotail observations, the 2-month red curve and the 6-year black dotted curve, have similar shapes. We regard the 6-year PDF as a robust sampling of the true velocity distribution in the central plasma sheet, and the extent of overlap indicates these 2 months reasonably approximate that true distribution. The short-duration, 2-month PDF (red) departs from the longer baseline behavior at fast tailward velocities, showing very few flows below -300 km/s, with an occurrence frequency $<4 \times 10^{-5}$. For most other speeds, the 2-month flow distribution well represents the baseline velocity distribution. The mean flows in the short and long Geotail data sets are similar: $\langle V_{Geotail, \, 2 \, mo.} \rangle = 16.1$ and $\langle V_{Geotail, 6 \, yr.} \rangle = 18.9$ km/s. For comparison, weak convection ($E_{SW} = 0.1$ mV/m) in the tail field ($\langle B_Z \rangle|_{X=-20} = 6.3$ nT) should drive $V_{PS} \sim E_{SW}/B_Z = 16$ km/s flows.

[15] The shape of the LFM PDF (blue curve) in Figure 3 resembles the observations (red, black curves) for slow, earthward flows, but has several distinct differences elsewhere. The LFM velocity distribution is significantly skewed toward earthward flows, like the observations, but it grossly underestimates the number of observed fast flows. Earthward flows >300 km/s and tailward flows <-50 km/s are conspicuously absent from the LFM PDF. The mean velocity ($\langle V_{\perp X} \rangle$) of the LFM distribution is 35.7 km/s, $\sim 2 \times$ larger than either PDF calculated from observations. This overestimate was found in global average velocity maps in a companion paper [*Guild et al.*, 2008] and is partially explained by the LFM overestimate of ionospheric transpolar potential. The results in Figure 3 show the average velocity overestimate is additionally due to the lack of appreciable tailward flows in the LFM plasma sheet. We determine why the LFM contains so few fast flows and even fewer tailward flows in the following section.

6.2. Resolution-Dependent Velocity Distributions

[16] We here investigate the lack of fast plasma sheet flows in the LFM model. In the interest of computational feasibility, we used the lowest resolution of the LFM model for the simulation described in this study. This low resolution led to computational cell sizes of $1 - 2 \, R_E$ in the plasma sheet. Large cell sizes generally limit plasma gradients in the model, leading to thicker current sheets, smaller $j \times B$ forces, and thus slower flows. We follow this line of

reasoning to determine how the flow distribution changes with simulation resolution as a potential explanation of our data/model discrepancy.

[17] We simulated a subset of our 2-month interval at high spatial resolution to compare with the velocity distribution determined with the low spatial resolution simulation. The high-resolution simulation had twice the number of computational cells in the azimuthal (θ) and polar (ϕ) coordinates, halving the cell size in those dimensions, while leaving the radial cell size unchanged. Increasing the resolution decreases the average plasma sheet cell size in the region $-30 < X_{GSM} < -10 \, R_E$ by 50%, from 1.36 to 0.90 R_E, so we expect the high-resolution model to support spatial gradients 50% larger as well.

[18] We simulated portions of the interval from 23 February through 22 March 1996 with the high-resolution model, outputing simulation results every 2 min. Again, this time resolution is sufficient to sample the smallest duration velocity structures contained in the simulations with statistical confidence. We simulated 21 d of the high-resolution model in total and show the PDFs of only those intervals common to both the low- (red) and high-resolution (blue) simulation in Figure 4. These PDFs are now composed of all plasma sheet velocities occurring between $-10 \leq X_{GSW} \leq -30 \, R_E$, rather than only those flows which intersect an orbiting spacecraft trajectory. Again, the LFM plasma sheet was defined as the set of points whose values satisfy all the criteria of Table 1 at every time step. We plot the velocity distribution observed during the entire 6-year Geotail data set in black for comparison, using $\Delta V = 20$ km/s for each PDF and extend the velocity limits to ± 1000 km/s for completeness. The average flow speed of all points in the low-resolution plasma sheet (15.4 km/s) differs markedly from the average flow speed along the Geotail orbit through that simulation (35.7 km/s), signifying the importance of orbital sampling when comparing temporally and spatially averaged quantities in the simulated plasma sheet. For the remainder of the study we compare only entire plasma sheet average flows.

[19] The distribution derived from all velocities within the low resolution plasma sheet (red PDF) now exhibits earthward flows up to 500 km/s and tailward flows up to 200 km/s. These faster flows were not present in Figure 3 and were missed due to the selective sampling of the Geotail orbit. The high-resolution PDF (blue curve) extends to $+650$ and -450 km/s, well above the fastest low-resolution speeds in each direction. Both simulated distributions still recorded much fewer fast flows than the observations, but increasing the resolution generated more fast flows, especially in the tailward portion of the distribution. These fast tailward flows in the high-resolution PDF also serve to reduce the average speed from 15.4 km/s in the low-resolution simulation to 11.3 km/s in the high-resolution simulation. Both distributions still fall well short of reproducing the number of very fast earthward flows and therefore underestimate the statistical Geotail average flow speed of 18.9 km/s. As the distribution indicates, rather than changing the typical flow speed, increasing the simulation resolution filled out the high-velocity tails symmetrically, reducing the average speed. We investigate
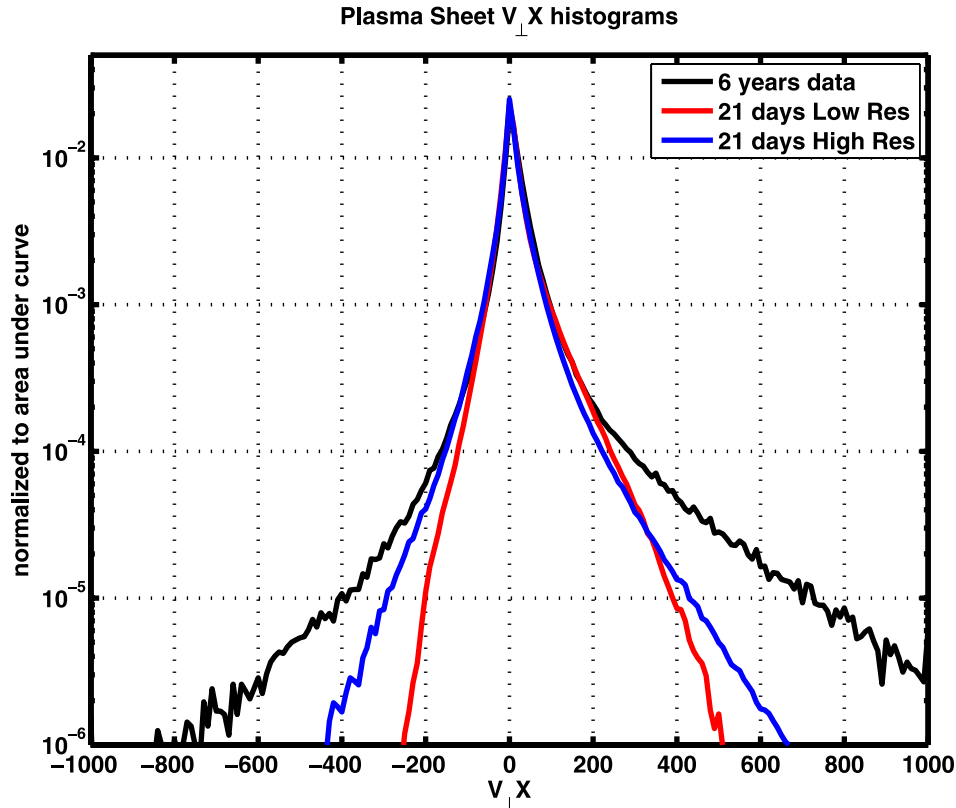
Plasma Sheet V$_\perp$X histograms

Figure 4. PDFs of the low- (red) and high-resolution models (blue), plotted together with Geotail data (black).

the cause of these additional fast flows in the following section.

7. Discussion

[20] The resolution-dependent nature of the LFM plasma sheet transport is not surprising, as increased resolution permits larger plasma gradients, which in turn can affect local dynamics. We work here toward understanding the mechanisms which add more, faster flows to the plasma sheet, as shown in section 6.2. For more insight, we turn to a time-dependent characterization of mass flux through a representative simulation at both resolutions.

[21] Instead of reanalyzing the high-resolution simulation in the time domain, we simulate a substorm which serves as a proxy for the dynamic intervals contained within the long simulation. Using WIND observations between 0600 and 0900 UT on 10 December 1996, we drove the substorm simulations using the low- and high-resolution LFM model. The high-resolution simulation was run and extensively compared to observations by *Wiltberger et al.* [2000] and yielded similar substorm onset times and magnetotail dynamics to in situ observations. The low-resolution simulation was performed for this study and uses identical upstream and ionospheric boundary conditions, restricting the only difference between comparative simulations to spatial resolution.

[22] The plasma sheet velocity PDFs for the high-resolution substorm simulation exhibited larger earthward and tailward fast flows in the tails of the distributions relative to the low-resolution simulation (not shown), similar to the

long-duration PDFs in Figure 4. During the course of the 2 1/2-h substorm simulation, we recorded the average mass flux ($\langle \rho \cdot V_X \rangle \cdot \sigma_{PS}$) through a 20×10 R_E ($Y_{GSM} \times Z_{GSM}$) surface centered at $(-20, 0, -4)$ R_E, accounting for the offset neutral sheet tailward of the magnetotail hinging distance in our December simulation. We assumed the mass density (ρ) consists of only protons and maintain constant surface area of the midtail surface (σ_{PS}) when computing the mass flux. We limited the $|Y_{GSM}|$ extent of the midtail grid to exclude any magnetosheath samples in our mass flux budget. Mass flux through this midtail surface was due to average trends of density or velocity, since the cross-sectional area remains constant. Also, the very low density characteristic of the lobes ensured most of the mass flux we tracked is from transport in the high-density plasma sheet. We averaged the (signed) mass flux through this surface at every simulation time step, for both simulation resolutions to characterize the plasma sheet mass transport as a function of simulation resolution. Differences in the resolution-dependent velocity PDFs in Figure 4 should thus be related to differences in plasma sheet mass transport between the two simulations.

[23] After extracting the average mass flux through the plasma sheet cross section from both simulations at every time step, we plot the cumulative mass flux in Figure 5. We normalize the total mass transported at the end of the substorm, as the mass flux through an arbitrary surface is a complex function of plasma sheet cross-sectional area and magnetotail geometry and is not necessarily a conserved quantity in this particular treatment. For this study, the relevant difference between the low-resolution (blue curve)

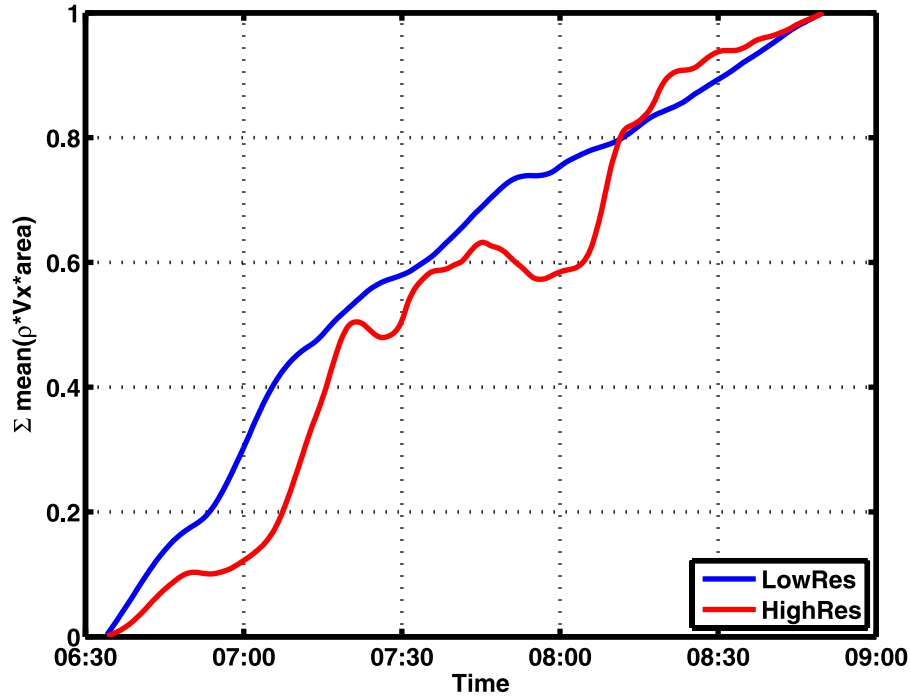**Normalized Mass Flux through the plasma sheet @ X_{GSM} = −20 during a substorm**

Figure 5. The cumulative mass flux through the X_{GSM} = −20 R_E cross section of the plasma sheet throughout a substorm simulation for the low- (blue) and high-resolution (red) models.

and the high-resolution mass flux (red curve) is the smoothness of the mass transport within the duration of the substorm. The high-resolution simulation possesses a far more variable mass transport than the low-resolution simulation. In fact, the high-resolution plasma sheet exhibits at least three intervals (near 0652, 0723, and 0750) of net tailward flow through the X_{GSM} = −20 surface, compared to a continuously increasing earthward mass flux in the low-resolution simulation. Accordingly, the low-resolution simulation seems to transport mass smoothly through the plasma sheet, whereas the high-resolution simulation transports mass in a bursty fashion.

[24] To emphasize this mass transport difference, we show equatorial planes of both substorm resolutions in Figure 6. Both Figures 6a and 6b show a view of the equatorial plane at Z_{GSM} = −4 R_E from the north, colored in terms of V_X from −500 (blue) to +300 km/s (red). The Sun is to the left, and black *GSM* coordinate axes have tick marks every 10 R_E. Both velocity maps were constructed from each substorm simulation at essentially the same time (within 3 s of each other). Therefore, simulation resolution is the only difference between Figures 6a and 6b, with the high-resolution simulation (Figure 6b) containing ∼4× more cells than the low-resolution simulation (Figure 6a).
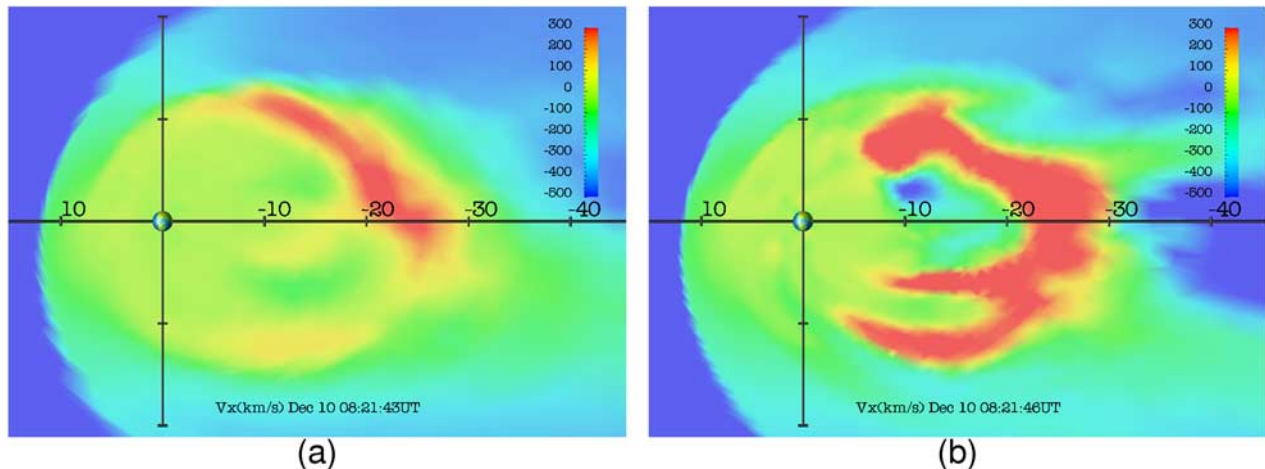

Figure 6. Equatorial planes of the (a) low-resolution and (b) high-resolution simulation colored from −500 (blue) to +300 km/s (red).

We selected these frames at 0821 UT, at a time when a significant neutral line developed in the midtail of both simulations, thereby organizing their subsequent dynamical evolutions. The high-resolution figure (Figure 6b) contains three channels of >300 km/s earthward flow which are limited in their Y_{GSM} extent. In contrast, the low-resolution simulation developed barely discernable channels due to their low flow speeds relative to the background flow. One representative "flow channel" in the high-resolution simulation was analyzed and discussed by *Wiltberger et al.* [2000], who suggestively compared these simulated features to bursty bulk flows [*Angelopoulos et al.*, 1994]. These simulated plasma sheet features typically exhibit much less complexity than corresponding fast flows in the observations, and this comparison will be the subject of a future publication. This inherently resolution-dependent nature of plasma sheet transport shown in Figure 6 explains the difference between velocity PDFs in Figure 4 and may partially explain the lack of fast flows in the low-resolution LFM PDF in Figure 3.

[25] The significant difference between the low- and high-resolution simulation in Figures 6a and 6b can only be due to simulation resolution, as mentioned above. In our case, however, simulation resolution can mimic differing physical processes when ideal MHD includes processes which turn on after a certain threshold stress has been reached (e.g., reconnection when the current sheet thins to within a grid cell). Although reconnection in the LFM is a purely numerical effect, decreasing the size of simulation grid cells in the tail can effectively decrease the minimum current sheet thickness which is stable to reconnection, increasing the amount of Maxwell stresses available to be dissipated through field reconfiguration. These dynamical changes accumulate in time throughout the simulation, to the point where each model solution state at a certain time depends on a complicated history of barely different events, yielding a diverging solution in time. The externally driven nature of the magnetosphere during times of increased activity tempers these accumulating deviations, and the results of this balance are illustrated in Figure 6.

[26] The above analysis shows how changing only the simulation resolution can significantly affect the realism of the plasma sheet flows, based on a comparison with the observed distribution of flows. The difference between the observations and simulations, however, are not limited to simulation resolution alone. Ideal MHD does not contain many of the relevant physical processes known to operate in the vicinity of thin current sheets and fast plasma sheet flows. Regardless of the simulation resolution, it likely does not realistically model the magnetic reconnection rate, nor does it include nonfluid dissipation or kinetic effects associated with reconnection. We can only quantify the effect of missing physics in the model when global simulations are "grid converged," or reach a solution which does not change with spatial resolution. The simulations presented here are not grid-converged, and we will investigate this further in a separate study.

8. Summary and Conclusions

[27] This study represents a new approach to global MHD model validation: using a long-duration simulation to test the statistical properties of the model against the statistical properties of observations in the plasma sheet. We compared bulk flow variability in the plasma sheet using a 6-year baseline of Geotail observations and 2 months of LFM simulations. Such long-duration simulations provide rigorous tests of global MHD models during routine conditions, and provide insight into systematic discrepancies uncovered in the comparison.

[28] We used probability density functions to characterize and compare the LFM plasma sheet flow variability with that observed by Geotail. In a direct comparison along the Geotail orbit, we found the lower-resolution LFM model grossly underestimates earthward flows >300 km/s and tailward flows <−100 km/s. The comparison improved significantly with increased simulation resolution, as the high-resolution model inherently transported mass through the plasma sheet via fast, bursty flows. This was likely due to better resolved thin current sheets which possessed greater localized Maxwell stresses capable of generating faster localized flows. These fast flows brought the velocity PDFs into closer agreement with the observations by extending the wings of the velocity distribution but were insufficient to completely resolve the discrepancy. Further investigations of grid convergence in global MHD models are outside the scope of this work, but will be a target of a future study.

References

Angelopoulos, V., et al. (1993), Characteristics of ion flow in the quiet state of the inner plasma sheet, *Geophys. Res. Lett.*, *20*, 1711–1714.

Angelopoulos, V., et al. (1994), Statistical characteristics of bursty bulk flow events, *J. Geophys. Res.*, *99*, 21,257–21,280.

Angelopoulos, V., T. Mukai, and S. Kokubun (1999), Evidence for intermittency in Earth's plasma sheet and implications for self-organized criticality, *Phys. Plasmas*, *6*, 4161–4168.

Baumjohann, W., G. Paschmann, and C. Cattell (1989), Average plasma properies in the central plasma sheet, *J. Geophys. Res.*, *94*, 6597–6606.

Baumjohann, W., G. Paschmann, and H. Luhr (1990), Characteristics of high-speed ion flows in the plasma sheet, *J. Geophys. Res.*, *95*, 3801–3809.

Borovsky, J. E., R. C. Elphic, H. O. Funsten, and M. F. Thomsen (1997), The Earth's plasma sheet as a laboratory for flow turbulence in high-[beta] MHD, *J. Plasma Phys.*, *57*, 1–34.

Borovsky, J. E., M. F. Thomsen, and R. C. Elphic (1998), The driving of the plasma sheet by the solar wind, *J. Geophys. Res.*, *103*, 17,617–17,640, doi:10.1029/97JA02986.

Guild, T., H. Spence, L. Kepko, V. Merkin, J. Lyon, and C. Goodrich (2008), Geotail and LFM comparisons of plasma sheet climatology 1: Average values, *J. Geophys. Res.*, *113*, A04216, doi:10.1029/2007JA012611.

Hnat, B., S. C. Chapman, G. Rowlands, N. W. Watkins, and M. P. Freeman (2003), Scaling in long term data sets of geomagnetic indices and solar wind ϵ as seen by WIND spacecraft, *Geophys. Res. Lett.*, *30*(22), 2174, doi:10.1029/2003GL018209.

Huang, C., and L. Frank (1994), A statistical survey of the central plasma sheet, *J. Geophys. Res.*, *99*, 83–95.

Kaufmann, R. L., W. R. Paterson, and L. A. Frank (2004), Magnetization of the plasma sheet, *J. Geophys. Res.*, *109*, A09212, doi:10.1029/2003JA010148.

Kennel, C. F. (1995), *Convection and Substorms: Paradigms of Magnetospheric Phenomenology*, *Int. Ser. Astron. Astrophys.*, vol. 2, Oxford Univ. Press, New York.

Kokubun, S., T. Yamamoto, M. Acuna, K. Hayashi, K. Shiokawa, and H. Kawano (1994), The Geotail magnetic field experiment, *J. Geomagn. Geoelectr.*, *46*, 7–21.

Lyon, J. G., J. A. Fedder, and C. M. Mobarry (2004), The Lyon-Fedder-Mobarry (LFM) global MHD magnetospheric simulation code, *J. Atmos. Terr. Phys.*, *66*, 1333–1350, doi:10.1016/j.jastp.2004.03.020.

Machida, S., Y. Miyashita, A. Ieda, A. Nishida, T. Mukai, Y. Saito, and S. Kokubun (1999), GEOTAIL observations of flow velocity and north-south magnetic field variations in the near and mid-distant tail associated with substorm onsets, *Geophys. Res. Lett.*, *26*, 635–638, doi:10.1029/1999GL900030.

Miyashita, Y., S. Machida, A. Nishida, T. Mukai, Y. Saito, and S. Kokubun (1999), GEOTAIL observations of total pressure and electric field variations in the near and mid-distant tail associated with substorm onsets, *Geophys. Res. Lett.*, *26*, 639–642, doi:10.1029/1999GL900031.

Mukai, T., S. Machida, Y. Saito, M. Hirahara, T. Terasawa, N. Kaya, T. Obara, M. Ejiri, and A. Nishida (1994), The low energy particle (LEP) experiment onboard the Geotail satellite, *J. Geomagn. Geoelectr.*, *46*, 669–692.

Nagai, T., et al. (1998), Structure and dynamics of magnetic reconnection for substorm onsets with Geotail observations, *J. Geophys. Res.*, *103*, 4419–4440, doi:10.1029/97JA02190.

Nishida, A., T. Mukai, T. Yamamoto, Y. Saito, S. Kokubun, and K. Maezawa (1995), GEOTAIL observation of magnetospheric convection in the distant tail at 200 R_E in quiet times, *J. Geophys. Res.*, *100*, 23,663–23,676, doi:10.1029/95JA02519.

Sorriso-Valvo, L., V. Carbone, P. Veltri, G. Consolini, and R. Bruno (1999), Intermittency in the solar wind turbulence through probability distribution functions of fluctuations, *Geophys. Res. Lett.*, *26*, 1801–1804, doi:10.1029/1999GL900270.

Tsyganenko, N. A., and T. Mukai (2003), Tail plasma sheet models derived from Geotail particle data, *J. Geophys. Res.*, *108*(A3), 1136, doi:10.1029/2002JA009707.

Wang, C.-P., L. R. Lyons, J. M. Weygand, T. Nagai, and R. W. McEntire (2006), Equatorial distributions of the plasma sheet ions, their electric and magnetic drifts, and magnetic fields under different interplanetary magnetic field B_z conditions, *J. Geophys. Res.*, *111*, A04215, doi:10.1029/2005JA011545.

Wiltberger, M., T. I. Pulkkinen, J. G. Lyon, and C. C. Goodrich (2000), MHD simulation of the magnetotail during the December 10, 1996, substorm, *J. Geophys. Res.*, *105*, 27,649–27,664, doi:10.1029/1999JA000251.

Wiltberger, M., R. S. Weigel, M. Gehmeyr, and T. Guild (2005), Analysis and visualization of space science model output and data with CISM-DX, *J. Geophys. Res.*, *110*, A09224, doi:10.1029/2004JA010956.

————————————

C. C. Goodrich, E. L. Kepko, J. G. Lyon, V. Merkin, and H. E. Spence, Center for Space Physics, Boston University, Boston, MA 02215, USA.

T. B. Guild, Space Sciences Department/Chantilly, The Aerospace Corporation, 15049 Conference Center Drive, CH3/210, Chantilly, VA 20151-3824, USA. (timothy.guild@aero.org)

M. Wiltberger, High Altitude Observatory, National Center for Atmospheric Research, 3450 Mitchell Lane, Boulder, CO 80301, USA.